Journal of ELECTRONIC MATERIALS, Vol. 38, No. 10, 2009 Regular Issue Paper
DOI: 10.1007/s11664-009-0877-1
© 2009 The Author(s). This article is published with open access at Springerlink.com

On the Mechanisms Governing Aluminum-Mediated Solid-Phase Epitaxy of Silicon

YANN CIVALE,[1] GUGLIELMO VASTOLA,[2] LIS K. NANVER,[1,4] RANI MARY-JOY,[1] and JAE-RYOUNG KIM[3]

1.—Laboratory of Electronic Components, Technology and Materials, Delft Institute of Microsystems and Nanoelectronics (DIMES), Delft University of Technology, Feldmannweg 17, 2628 CT Delft, The Netherlands. 2.—L-NESS and Department of Materials Science, Milano-Bicocca University, Via R. Cozzi 53, 20125 Milan, Italy. 3.—Molecular Electronics and Devices, Kavli Institute of Nanoscience Delft, Delft University of Technology, Lorentzweg 1, 2628 CJ Delft, The Netherlands. 4.—e-mail: L.K.Nanver@tudelft.nl

Mechanisms governing the aluminum-mediated solid-phase epitaxy of Si on patterned crystalline Si substrates have been identified by studying the deposited material as a function of growth conditions when varying parameters such as temperature, growth time, and layer-stack properties. Early growth stages can be discerned as first formation of "free" Si at the Al/α-Si interface, then diffusion of Si along the Al grain boundaries, nucleation at the Si substrate surface, nuclei rearrangement, and finally crystal growth. The acquired understanding is applied to control the selectivity and completeness of single-crystal growth in various sizes of contact windows to the Si substrate.

Key words: Aluminum doping, aluminum-induced crystallization, layer-exchange mechanisms, low-temperature doping, p^+–n diodes, silicon crystal growth, silicon epitaxy, solid-phase epitaxy

INTRODUCTION

Today low-temperature silicon crystallization techniques are receiving a lot of attention because of the potential for fabricating electronic semiconductor device building blocks for applications such as thin-film transistors, solar cells, and semiconducting nanowires. In particular, mechanisms leading to the formation of polycrystalline silicon thin films have been investigated intensively over the past few years. The crystallization of amorphous silicon (α-Si) can be driven by a reduction in Gibbs free energy, a process that can be energetically enhanced by the presence of a metal layer such as nickel (Ni)[1] or aluminum (Al)[2]. For example, the activation energy for solid-phase crystallization of α-Si of about 2.7 eV[3] is reduced to about 0.8 eV when the semiconductor is in contact with Al.[4] A generally accepted mechanism of crystallization based on α-Si/Al layer exchange has been used to describe the growth of polycrystalline Si on foreign substrates in this situation.[5–7]

In previous studies,[8,9] we reported a sub-500°C selective Si solid-phase epitaxy (SPE) process using Al as a transport medium. On both patterned and nonpatterned crystalline Si substrates this process produced high-quality monocrystalline Si (c-Si) islands, which are uniformly doped with Al.[10] Focus was placed on the use of these p^+ SPE-Si islands for the fabrication of devices containing p^+–n diodes and p^+ contacts. Device quality was found to be exceptionally good for a large range of device geometries and process parameters, including temperatures down to 400°C.

In this study, the focus is on the mechanisms that govern the SPE-Si growth. An intensive study of the earliest growth stages and the dependence on the Si substrate orientation has been carried out, on the basis of which a semi-empirical growth model is proposed. Particularly, the time and substrate dependence of SPE-Si coverage is addressed in this

(Received May 19, 2008; accepted June 11, 2009; published online July 7, 2009)

study, as well as the fabrication parameters affecting the controllability of the selective growth. It is shown that the latter can be optimized for the selective filling of a wide range of geometries. In particular, the electrical characterization of SPE-Si based p^+n ring-shaped diodes as large as 1 μm × 395 μm is presented.

EXPERIMENTAL PROCEDURES

In one group of experiments, SPE was performed on bare Si wafers with (100), (110) or (111) orientation. In most of the experiments, (100)-Si substrates were patterned by first growing 30 nm of thermal silicon dioxide (SiO_2) in which contact windows to the Si are etched. In all cases, the preparation of the samples for the SPE growth sequence is as follows: the Si surface was first cleaned in a nitric acid solution (HNO_3) and the resulting native SiO_2 was removed by dip-etching in diluted hydrofluoric acid (HF) 0.55% for 4 min. This provides hydrogen-terminated surface passivation. Directly after dip-etching, wafer rinsing, and drying, a layer stack of Al (containing 1 at.% Si) and α-Si was formed by physical vapor deposition (PVD) at 50°C.

Both PVD depositions were performed using an argon flow of 100 sccm and without breaking vacuum so that the formation of an insulating native aluminum oxide (Al_2O_3) layer before the α-Si deposition was prevented. The influence of an Al_2O_3 layer between the PVD thin films has already been investigated by many research groups for the case of aluminum-induced Si crystallization on SiO_2. Particularly, Schneider et al.[11] showed that the presence of such an insulating interface affects the growth by introducing a diffusion barrier to Si transport. This yields a slower Si crystallization process, resulting in the formation of larger polycrystalline Si islands. The influence of such Al_2O_3 layers was not investigated in this study.

The bulk of the results presented herein correspond to thicknesses of the deposited Al and α-Si thin films of 200 nm and 20 nm, respectively. On the samples with contact windows through the oxide, the layer stack was patterned so as to cover the contact windows and extend around them by varying amounts, as shown in Fig. 1. The samples were then transferred to the annealing module, in which a thermal treatment in argon was performed at either 400°C or 500°C. After annealing, the Al layer was removed selectively to Si and SiO_2, using a conventional metal-etchant solution. The as-obtained surfaces were then analyzed by scanning electron microscopy (SEM) in order to identify the successive stages of the growth sequence and determine the dependence of the SPE-Si surface coverage on parameters such as the growth time, the Si source composition, and the substrate orientation.

In some cases, the p^+ SPE-Si islands were grown on n-type substrates so as to form p^+n junctions. The anode and cathode (back of the wafer) were contacted by PVD deposition of Al/(1% Si) and interconnect patterning on the front of the wafer as described in previous publications.[8]

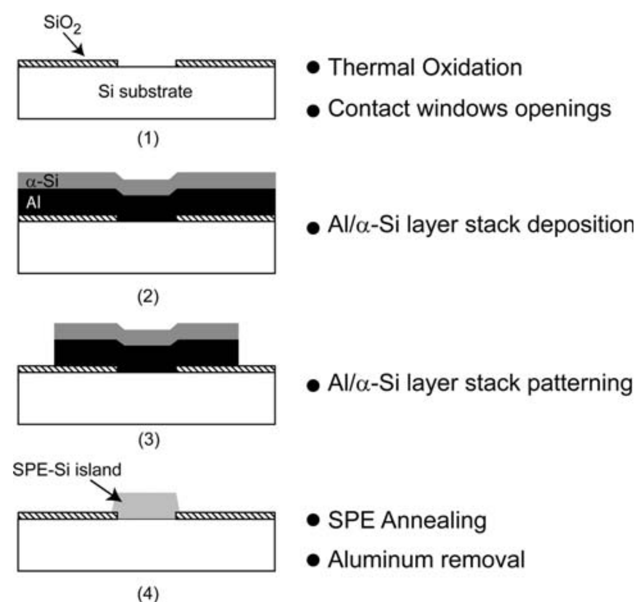

Fig. 1. Schematic process fabrication flow for the SPE-Si growth test structures. Contact windows are patterned and etched through thin (30-nm) thermally grown SiO_2 to the Si substrate.

BASIC GROWTH MECHANISMS

Basic Growth Sequence

A series of SEM images that illustrate the different stages of the SPE crystal growth are shown in Fig. 2. From this type of experimental observation, it has been possible to conclude that the growth sequence is composed of the following consecutive steps: (1) formation of "free" Si at the Al/-Si interface, (2) diffusion of Si along the Al grain boundaries, (3) nucleation at the Si substrate surface, (4) nuclei rearrangement, and (5) crystal growth. Each of these stages is specified in Fig. 3 and addressed below in detail.

Formation of "Free" Si Atoms

As described by Hiraki's[12] model, free electrons in the Al layer adjacent to the α-Si first screen the Si covalent bonding and thus weaken the Si-Si bonds. The relatively weakly bonded Si atoms are called "free" Si because of their ability to migrate through the Al layer. It is generally accepted that such a screening effect only acts over a short range and will be restricted to the first two atomic monolayers of the α-Si layer. The formation of such "free" Si atoms is indirectly substantiated by the experimental observation that, after long-term annealing of the Al/α-Si layer stack, all that remains is a surface coverage of Al on the test structures, i.e., the deposited α-Si has dissolved and diffused through the metal film.

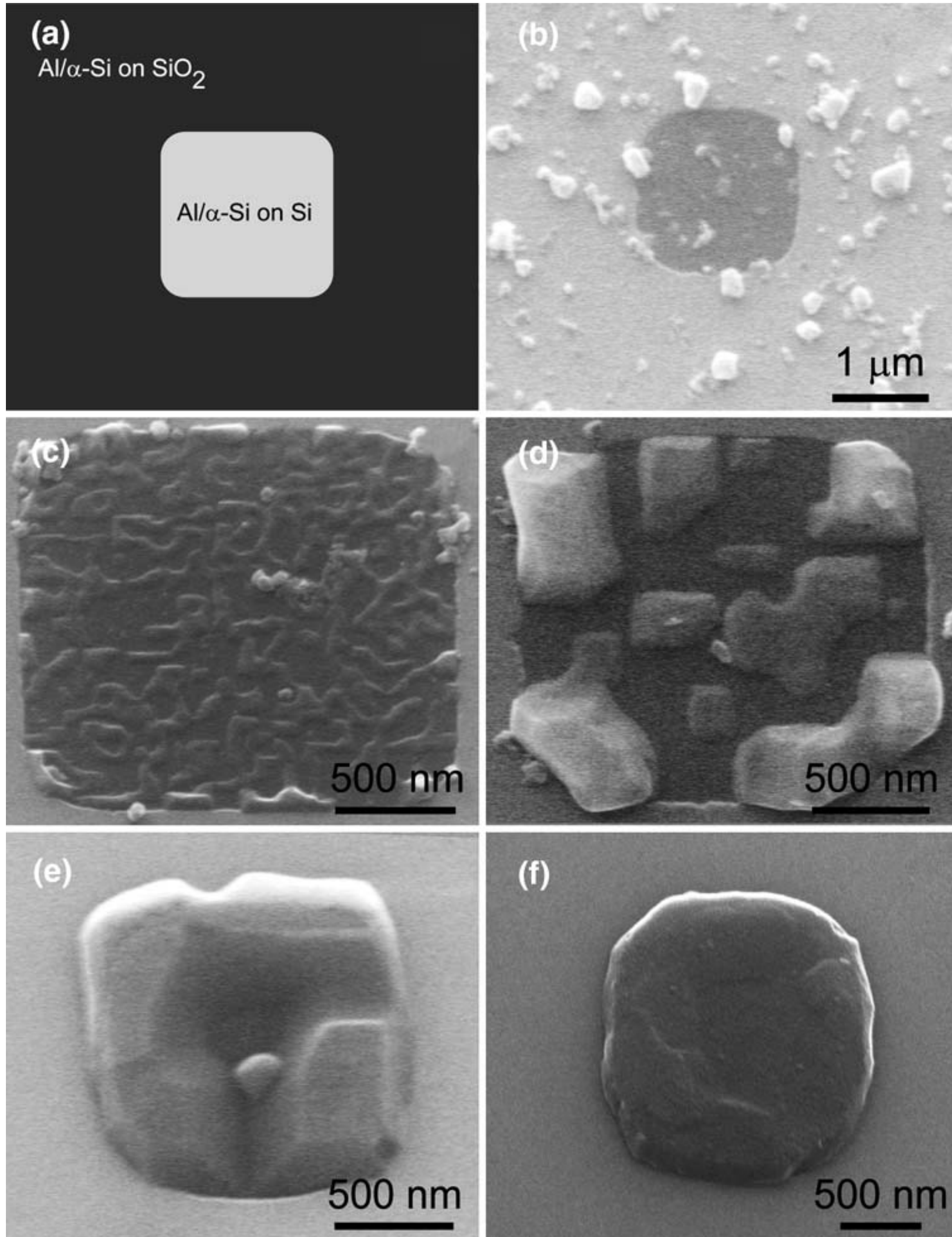

Fig. 2. (a) Schematic top view of the contact window (light-grey region) before SPE-Si growth. After the SPE growth and Al removal, SEM micrographs of the contact window region were analyzed after different growth times and temperatures: (b) 1.5 min at 500°C, (c) 2 min at 400°C, (d) 6 min at 500°C, (e) 30 min at 500°C, and (f) 30 min at 500°C. In the latter case, an optimal Al/α-Si layer stack geometry and thickness ratio has been used to obtain near-ideal growth selectivity.

Diffusion Through the Al Grain Boundaries

The Al layer, deposited by PVD at 50°C, is microcrystalline and contains a high density of grain boundaries.[13] Thus, Si can diffuse either: (1) through the Al grains, (2) along the Al grain boundaries, (3) along the Al to the α-Si interface or (4) along the Al to the Si-substrate interface. The diffusion path along the Al grain boundaries is known to be predominant in the early stages of thermal treatment of Al/Si alloys.[14] Thermodynamically, the occurrence of Si diffusion along the Al grain boundaries is governed by the difference between the interface energies as given by

$$2 \cdot \gamma_{\langle \mathrm{Al} \rangle - \{\mathrm{Si}\}} - \gamma_{\langle \mathrm{Al} \rangle} \quad (1)$$

where $\gamma_{\langle \mathrm{Al} \rangle - \{\mathrm{Si}\}}$ is the interface energy between the Al and α-Si layers and $\gamma_{\langle \mathrm{Al} \rangle}$ is the grain boundary energy of Al. Following methods previously reported by Wang et al.,[5] $\gamma_{\langle \mathrm{Al} \rangle - \langle \mathrm{Si} \rangle}$ and $\gamma_{\langle \mathrm{Al} \rangle}$ were calculated at 500°C, and found to be 2.85×10^{-2} J m^{-2} and 3.5×10^{-1} J m^{-2}, respectively. This establishes that there is a positive driving force for the inward

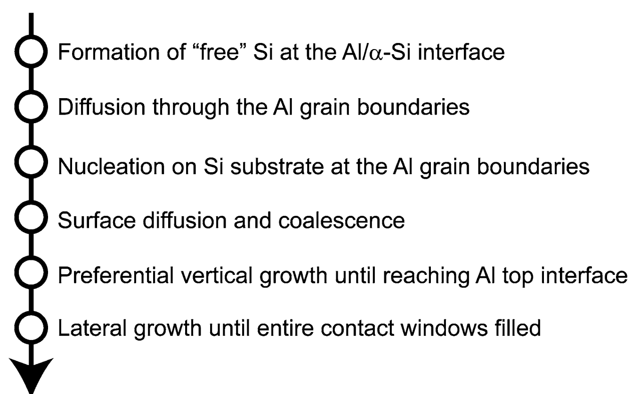

Fig. 3. The SPE-Si growth sequence.

diffusion of Si along the Al grain boundaries. A preference for the diffusion of Si along the Al grain boundaries is manifested by the shape and overall pattern of the deposited Si in the coalescence stage discussed below.

Nucleation and Coalescence

He et al.[15] reported the existence of a critical Si thickness, h_c, above which Si crystallizes. The value of h_c depends on the crystallization energy of α-Si, $\Delta G_{\langle Si\rangle-\{Si\}}$, and on the interface energy of Al with respect to the amorphous and crystalline Si interface, $\gamma_{\langle Al\rangle-\{Si\}}$ and $\gamma_{\langle Al\rangle-\langle Si\rangle}$, respectively, as given by the relationship

$$h_c = \frac{2 \cdot \left(\gamma_{\langle Al\rangle-\langle Si\rangle} - \gamma_{\langle Al\rangle-\{Si\}}\right)}{-\Delta G_{\langle Si\rangle-\{Si\}}}. \quad (2)$$

In our case h_c is about 0.56 nm, which corresponds to approximately 2.5 atomic monolayers, i.e., it is much smaller than the thickness of the deposited α-Si thin film. Accordingly, α-Si does not remain in a stable amorphous phase at the grain boundaries and will crystallize upon reaching the Si or oxide surface. This nucleation stage of the growth process was observed in our experiments after an annealing time of 1.5 min at 400°C. It is characterized by a fine distribution of deposited Si nuclei, the shape of which displays no preferential orientation, both on the Si substrate and the oxide as illustrated by Fig. 2b.

As the Si diffusion along the grain boundaries progresses, both the number and the size of the Si nuclei increases until they impinge upon each other and merge. At 400°C, the diffusion process is slow enough to allow the intermediate coalescence stage to be observed. This is shown in the SEM image in Fig. 2c, where the nucleated islands have coalesced to form a liquid-like pattern[16] that follows the Al grain boundaries. This reflects the predominance of the diffusion along the Al grain boundaries in the early stages of the growth process, as predicted by Eq. 1.

Growth on Nonpatterned Substrates

After nuclei coalescence, larger Si crystals will form because the formation of additional Si-Si bonds corresponds to a lowering in energy. Quantitatively, this energy gain corresponds to the energy necessary for a new Si facet to be attached to the already formed Si crystal. To do so, four new Si-Si bonds have to be formed per unit cell. By the use of the binding energy given by the Tersoff potential[17] for bulk Si of about −4.62 eV, and assuming a facet width of 0.54 nm, the energy gain corresponding to the formation of a new SPE-Si facet is approximately $-2.5\ \mathrm{J\ m^{-2}}$, which is much larger than the gain in energy from the formation of a Si-to-Al interface bond. This also means that there will be a tendency for the system to form large crystals since the free energy per atom (or per unit volume) decreases as the crystal volume increases.

The influence of the substrate orientation on the SPE has been investigated in the literature and a few already proposed models have demonstrated that the fastest growth rate is along the ⟨100⟩ directions.[18] In particular, Drosd and Washburn[19] formulated that the main criterion for Si in the amorphous phase to crystallize is the formation of at least two undistorted bonds with the crystal. On the basis of geometrical considerations, it can be concluded that this requirement is easily met in the (100) plane because one incoming Si atom can establish the necessary bonds. Along the (110) or (111) planes, however, the growth will be much slower because the bonds can only be achieved by the formation of a cluster of either two or three atoms, respectively. Several of our experiments reveal behavior that can be well understood in terms of this crystal growth criterion and they are described below.

Figure 4 shows SEM images of the results of SPE growth on nonpatterned substrates with an orientation of either (100), (110) or (111) as obtained after annealing at 400°C for 30 min. The analysis of the (100) substrate after growth and Al removal shows that the SPE forms rectangular Si islands with sides parallel to the ⟨110⟩ directions and with a height equal to that of the originally deposited Al layer, as shown in Fig. 4a. This is in agreement with a fastest growth rate in the ⟨100⟩ directions because the direction perpendicular to the Si substrate surface is a ⟨100⟩ direction. Moreover, according to the well-established Wulff theory, the final shape of a growing crystal is determined by the slowest growth direction.[20] Thus, the fact that ⟨110⟩ facets are exposed in the final growth stage also indicates a slower growth in the ⟨110⟩ than in the ⟨100⟩ direction. Most islands look square-like as would be expected from growth rate considerations, but a few are rectangular. This is feasibly connected to the varying accessibility of the sides with respect to the supply of silicon during growth of the crystal itself and the crystals in the vicinity.

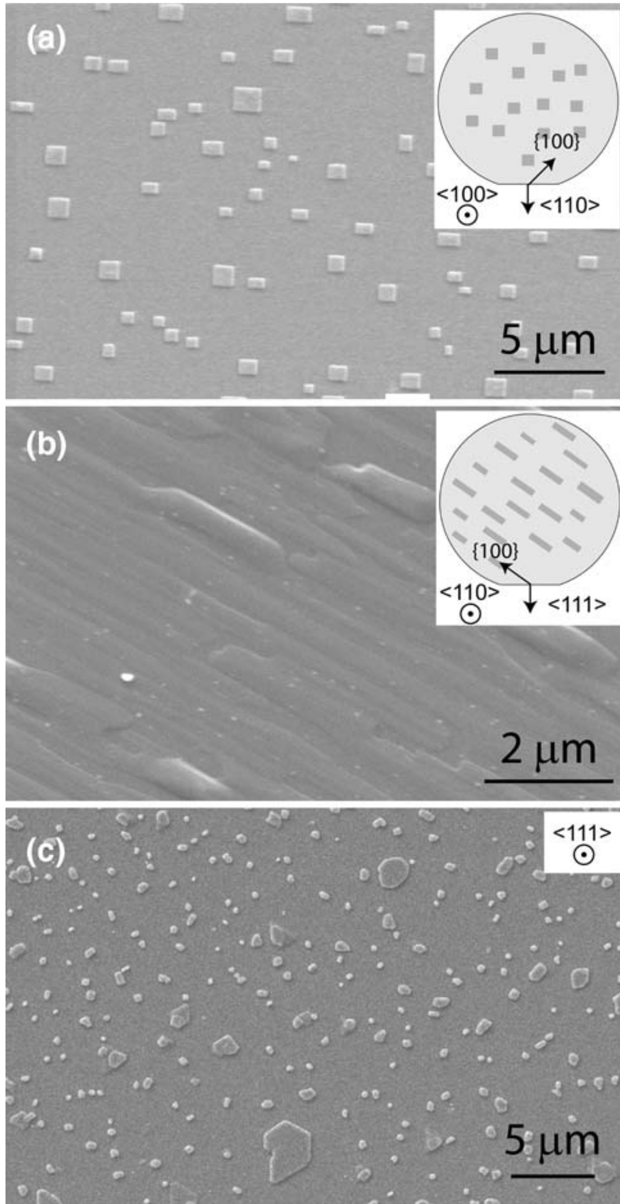

Fig. 4. Bare-Si substrate surface after SPE-Si growth and Al removal in the case of: (a) a (100)-oriented Si substrate, (b) a (110)-oriented Si substrate, and (c) a (111)-oriented Si substrate. In all cases, the growth temperature was 400°C, the annealing time was 30 min, and the Al and α-Si thin film thicknesses were 200 nm and 20 nm, respectively.

When the total surface occupied by SPE-Si islands is integrated for the situation shown in Fig. 4a and the island height is assumed to be within 7% of the deposited Al thickness, a total volume is found that corresponds well to the deposited volume of α-Si. This agrees with the view that practically all the deposited α-Si is crystallized by SPE. The vertical growth apparently stops when the SPE-Si height has reached the initial Al layer thickness. This feature will be addressed in more detail in the following section.

The results obtained on (110)-oriented substrates, illustrated in Fig. 4b, show discontinuous but micron-long stripe-like structures growing along the $\langle 100 \rangle$ direction and essentially covering the whole of the sample surface. The height of these structures is a few tens of nanometers, which is far smaller than the 200 nm Al layer. Therefore, it would appear that the fast growth in the $\langle 100 \rangle$ direction has exhausted the supply of Si at the cost of the slower vertical growth in the $\langle 110 \rangle$ direction. Electron backscattering diffraction analysis was performed on the (100)- and (110)-oriented Si samples and it was confirmed that the epitaxially grown Si preserves, in both case, the orientation of the substrate. The difference in shape of the SPE regions obtained on (100)- and (110)-oriented substrates (squares and rectangles, respectively) can be understood in terms of the balance between Si/Al interface energy and the Al grain boundary energy. The vertical growth of c-Si on (100) samples involves the formation of four new Si(110)-to-Al interfaces. Keeping in mind relationship (1), the following relation holds:

$$4 \cdot \gamma_{\langle(110)-\mathrm{Si}\rangle-\langle\mathrm{Al}\rangle} - \gamma_{\langle\mathrm{Al}\rangle} < 0. \qquad (3)$$

In contrast, the rectangular-shaped islands observed on Si(110) wafers tend to grow laterally rather than vertically: since this mechanism involves the creation of only two new Si-to-Al interfaces, it is an indication that relation (1) is here restricted to

$$2 \cdot \gamma_{\langle(100)-\mathrm{Si}\rangle-\langle\mathrm{Al}\rangle} - \gamma_{\langle\mathrm{Al}\rangle} < 0. \qquad (4)$$

On the (111)-oriented substrate (Fig. 4c), only $\langle 111 \rangle$ directions are available on the surface. Many structures, particularly the small ones, are irregular and do not exhibit any clear preferential growth directions. The density of islands is much higher and the average island surface area much smaller than for the (100)-substrate situation. This inadequate ability to coalesce into larger crystals is a clear indication that growth in the $\langle 111 \rangle$ direction is difficult to initiate. However, island growth similar to that observed on the (100) sample is sporadically observed and a few large micron-sized islands can be found. For these it is possible to identify a preference for forming triangular-like shapes incorporating 120° angles and a preferred growth from the corners of the crystals in the three $\langle 111 \rangle$ directions. These larger islands have a height of $\sim$180 nm, which is in good agreement with the targeted thickness of the deposited Al/(1% Si) layer, i.e., 200 nm.

Growth on Patterned (100) Substrates

When SPE-Si islands are formed locally in contact windows, the mechanisms governing the SPE growth remain the same as for bare Si. However, as seen in the SEM micrograph presented in Fig. 2d, the crystals grow predominantly at the contact

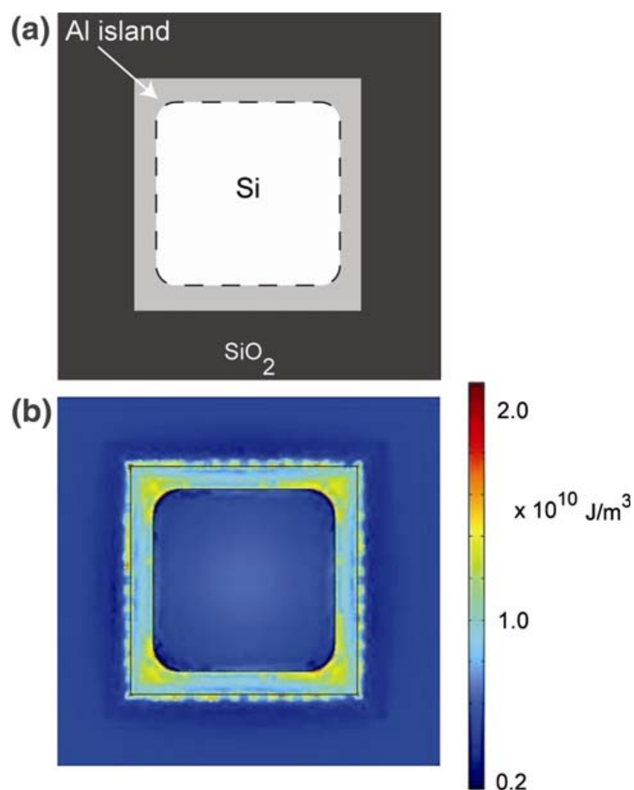

Fig. 5. FEM results showing the strain distribution in the Al thin film covering the contact windows opened through oxide, in the case of a fully strained Al thin film.

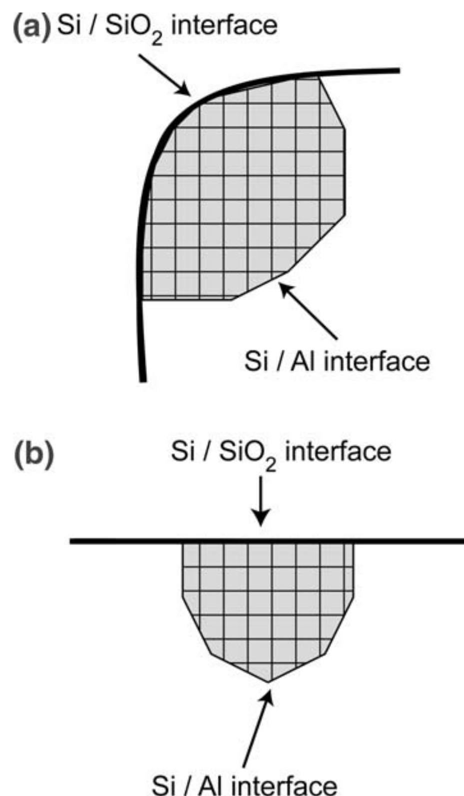

Fig. 6. Schematic of the SPE-Si deposition within the contact window: (a) at a corner and (b) along one of the sides. In both cases, the length of the SPE-Si/Al interface is identical.

window perimeter. To evaluate whether this effect could be stress induced, finite-element modeling analysis was performed to evaluate the strain distribution in the as-formed SPE-Si/SiO_2/Al structure. The results, illustrated in Fig. 5, indicate a reduction of the Al thin-film elastic energy field by a partial transfer of deformation to the oxide along the edges of the contact window. If it is assumed that the incoming Si is kinetically capable of traveling across the whole Al-to-Si window surface, the SiO_2/Si interface would correspond, from a lattice deformation point of view, to a local minimum of the Si chemical potential found in the contact window,[21] and this results in a preferential diffusion direction for the Si atoms. Moreover, the nucleation of c-Si at the window perimeter corresponds to the substitution of an SiO_2/Al interface with an SiO_2/SPE-Si plus an SPE-Si/Al interface. The corresponding surface energies are $0.15\ J\ m^{-2}$ and $0.3\ J\ m^{-2}$, respectively.[22] Since the SiO_2/SPE-Si interface is lower in energy than the SPE-Si/Al interface, it is natural for the system to try to maximize the exposure of the SiO_2/SPE-Si interface per unit volume, as illustrated in Fig. 6. Thus, it clearly follows from geometrical considerations that the deposition of Si at the corners of the contact windows is favorable.

As also observed on the nonpatterned samples, the SPE-Si island thickness is accurately controlled by the height of the initial Al layer. If the growth of the SPE crystal was not limited in height by the Al layer, multifaceted crystals would be expected to grow in the manner that is commonly observed for other conventional Si epitaxy techniques. This has in fact been observed in the situation where the SPE growth is limited by the supplied Si and not the Al thickness. An example is shown in Fig. 7a where a 200-nm-wide contact window is filled by the Si supplied from a 200-nm-thick Al/(1% Si) layer.

When a sufficiently large amount of Si is supplied, the vertical growth of SPE-Si, in the case of both bare Si and patterned samples, stops abruptly when the SPE-Si island reaches the thickness of the initial Al, the multifaceting is inhibited and rectangular crystals form, among which the larger ones are very close to being perfect squares. This is in agreement with the results previously reported by Nast and co-authors[24,25] for a layer-exchange aluminum-induced crystallization mechanism on glass substrates. During the SPE process, the Al film is segregated above the SPE-Si and forms an amorphous-like film like the one shown in Fig. 7b. The Al has a porous composition, very different from the polycrystalline Al composition of the Al in the original Al/α-Si layer stack. The results indicate that the Al that is segregated above the SPE-Si is no longer able to act as a transport layer for SPE

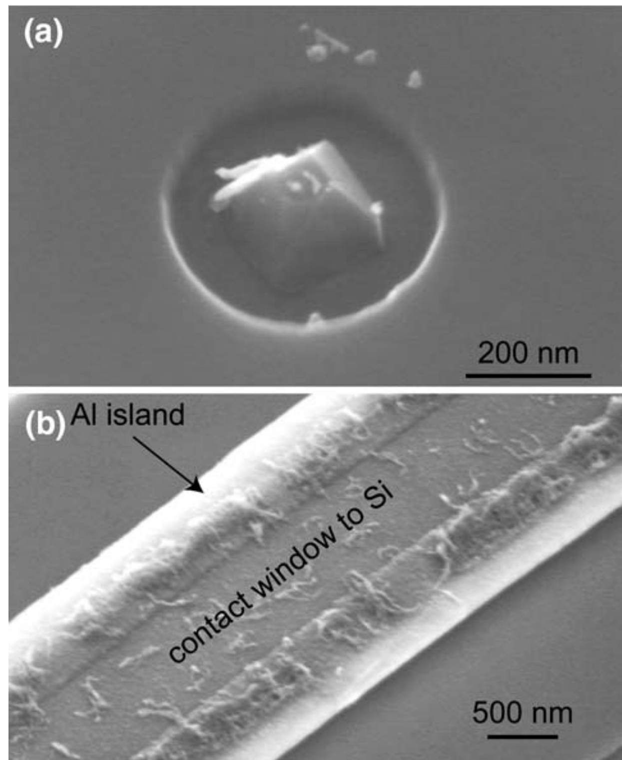

Fig. 7. (a) SEM micrograph of a 200 nm × 200 nm contact window filled in with a faceted SPE-Si island. These dimensions were achieved by using a silicon nitride spacer technology.[23] The source of Si was limited to the Si from a 200-nm-thick Al(1% Si) layer. (b) SEM micrograph of a contact window after being entirely filled with SPE-Si, and before the Al layer removal.

growth. Thus the SPE growth is terminated when the vertical growth of SPE-Si brings the Si into contact with the porous Al.

Due to the low thickness of α-Si used in our case (only 10% of the Al thickness), the SPE-Si growth is rapidly fed from the sides by diffusion of dissolved Si through the Al layer. While the Si diffuses through the Al grains, the Al is segregated on top of the grown SPE-Si island. Thus, supplying thicker α-Si or wider α-Si islands does not help to form a thicker thin film, since the SPE-Si island height is truncated when it reaches the initial Al layer thickness. The growth is stopped vertically and eventually tooth-like SPE-Si islands are formed, an example of which is shown in Fig. 2e. A very slight dent is observed in the middle of the island shown in Fig. 2f, which shows otherwise complete filling of the SPE window. Such a dent can be the result of the original Al topography or due to a lack of Si reaching the center of the structure. This may occur if the supply of Si from the sides is cut off by a completed vertical growth at the window perimeter or if too much Si crystallizes on the oxide rather than migrating to the contact window. The latter can be the result of nucleation on the dielectric or due to some measure of lateral overgrowth of the oxide from the SPE-filled contact window perimeter.

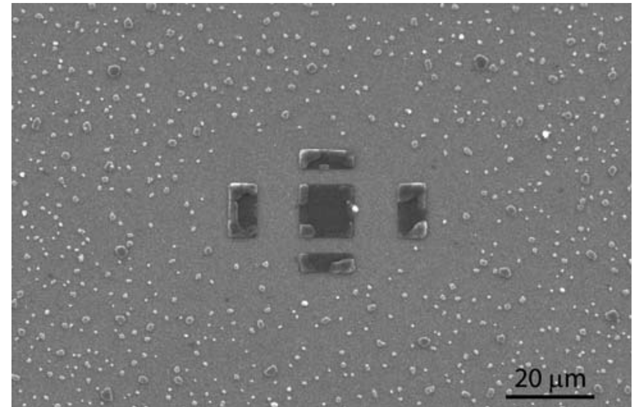

Fig. 8. SEM micrograph of five contact windows after 30 min growth at 500°C showing the preferred deposition on the Si in the contact windows.

As far as the Si nuclei on the oxide surface are concerned, they do not play a role as long as the Si is supplied close to the contact window and it is given time enough to diffuse to the contact window. The high diffusivity of the Si on the oxide can be observed indirectly as a reduction of the Si nuclei density on the exposed oxide surrounding the contact windows as the growth time increases. In Fig. 8 the situation for four neighboring contact windows covered by a nonpatterned Al/α-Si layer stack is shown. After a 30 min anneal at 500°C, about a 7-μm-wide oxide region directly around the contact windows is free of Si nuclei.

Surface Area Coverage

The coverage of a contact window with SPE-Si as a function of annealing temperature and time was extracted from SEM images. The results are plotted in Fig. 9a for different Al/α-Si layer stack areas. Two distinct regions can be identified: first the SPE-Si coverage increases as the annealing time increases, which can be correlated to the growth behavior during the nucleation and the coalescence stages. Then the coverage remains constant (or slightly decreases) with further increase of the annealing time. This is accompanied by an increase in vertical growth, so the volume of deposited SPE-Si does significantly increase when the growth time is prolonged. This is in accordance with the drive to form compact structures and the fact that growth will preferably take place in the ⟨100⟩ vertical direction perpendicular to the Si substrate surface. A constant coverage as a function of time is observed until the vertical growth is completed, i.e., when the SPE-Si island height reaches the thickness of the initial Al transport layer. At that moment the coverage starts to increase with time because the lateral growth on the Si and possibly also overgrowth of the oxide become predominant.

The SPE-Si coverage as a function of the width of the Al/α-Si layer stack area for an annealing time of

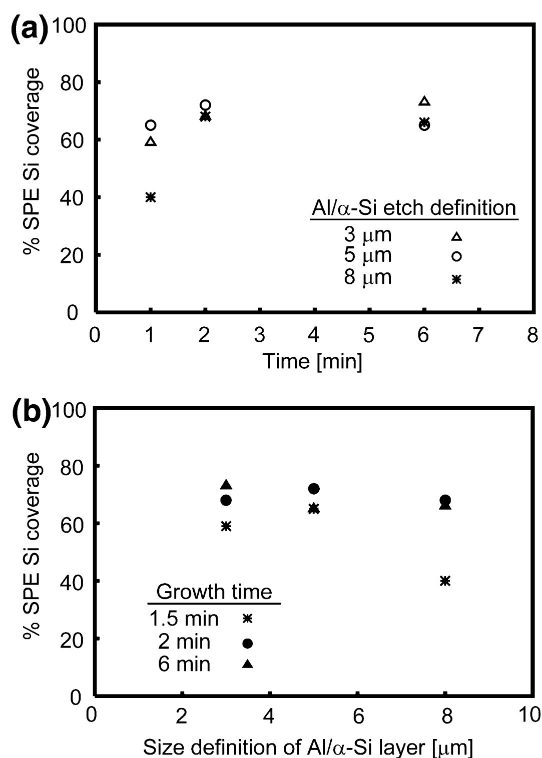

Fig. 9. Coverage of contact windows with SPE-Si as a function of (a) annealing time, and (b) Al/α-Si island area.

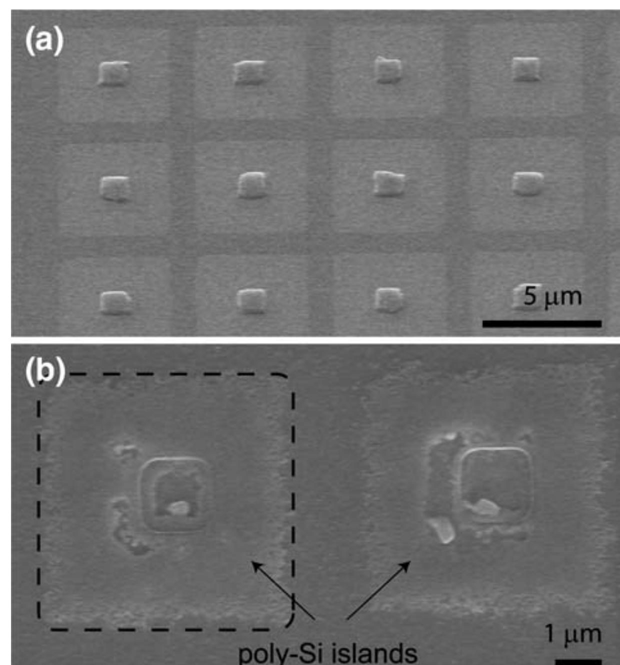

Fig. 10. SEM micrograph of contact windows to Si through: (a) thermal SiO_2 grown at 850°C, (b) PECVD SiO_2 deposited at 400°C; after SPE of enough Si to fill the windows completely. The dashed line in (b) represents the original Al/α-Si layer stack area, which in both images can be discerned as a ~5 μm × 5 μm light-grey area around the 1 μm × 1 μm large contact windows. In all cases, the Al transport layer has been removed selectively to SiO_2 and Si.

either 1.5 min, 2 min, or 6 min is also plotted in Fig. 9b. The coverage is found to be nearly constant, irrespective of the Al/α-Si area. However, even though the surface coverage is nearly constant, the volume of created SPE-Si increases with the Al/α-Si area. This effect is related to the ability of the Si nucleated on the oxide to diffuse to the contact window. For the smallest Al/α-Si area (3 μm × 3 μm), the region around the contact windows is smooth and apparently Si-free, indicating that the entire α-Si layer has contributed to the vertical growth within the contact window. When the initial Al/α-Si area is much larger than the contact window, Si nucleation on oxide is observed for short growth times. In this case, the ratio of Al/α-Si layer to exposed oxide area is apparently so large that there is a significant probability that energetically favorable defects in the thermal oxide are found and given occasion to function as nucleation centers for the “free” Si atoms. Isolated polycrystalline Si islands can then grow. This will be discussed further in the following section. In general, it can be concluded that, if selective filling of the contact window is desired, the amount of exposed oxide surface should be as limited as possible. After a sufficiently long annealing time, typically 30 min for the 400°C anneal, the lateral growth progresses until the entire window surface is covered, provided that the α-Si layer is thick enough to supply the necessary Si.

PROCESS PARAMETER CONSIDERATIONS

Influence of the Dielectric Surface Properties

It was shown above that the Si migration along the surface of the dielectric during SPE gives the mobile Si the chance to reach the window to the Si substrate and preferably crystallize there. Defects in the oxide film surface can function as preferred nucleation centers for the SPE-Si growth process, and thus the quality of this dielectric also plays a role in controlling the growth in the contact windows. The very high selectivity achieved for the sample shown in Fig. 10a was obtained by using SiO_2 thermally grown at 850°C with a low defect density. In this case there is a practically ideal selective deposition of SPE-Si on the c-Si surface rather than the oxide surface. In contrast, if a plasma-enhanced chemical vapor deposition (PECVD) of SiO_2 performed at 400°C is used, the situation is reversed. As can be seen in the example shown in Fig. 10b, very little SPE-Si is deposited in the contact windows and the available Si has been consumed by the deposition of polycrystalline Si on the oxide. This type of oxide apparently has a surface structure that provides a dense distribution of nucleation sites for the incoming Si that is therefore largely prevented from diffusing to the contact window. This is substantiated by previously reported atomic force microscopy analysis showing

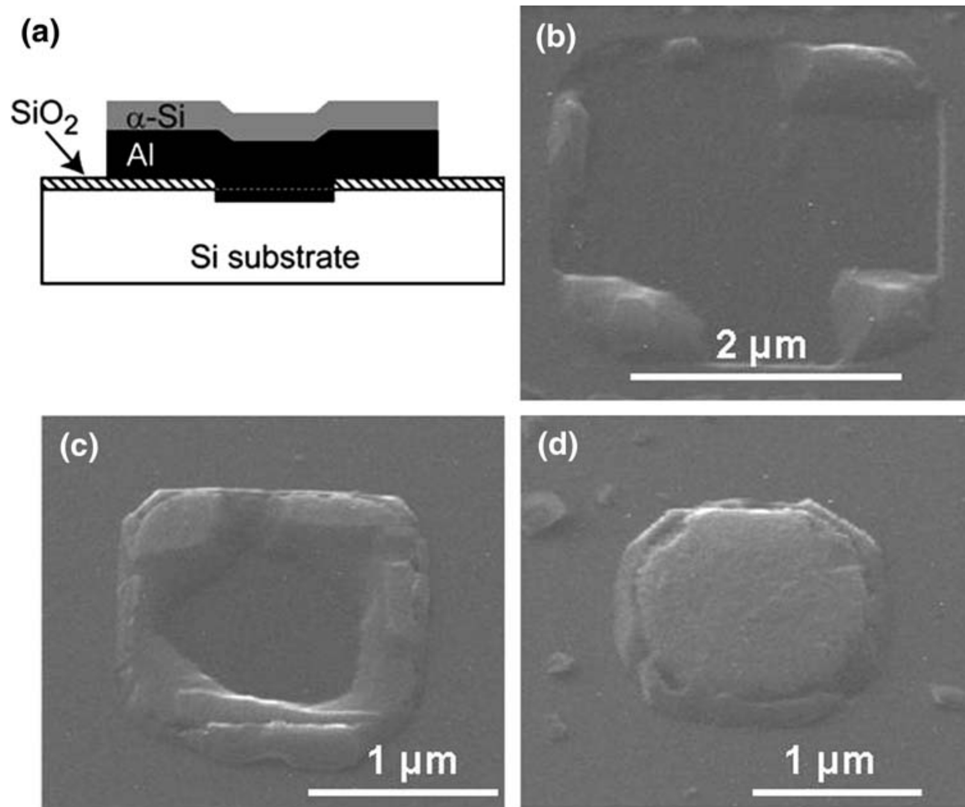

Fig. 11. (a) Schematic cross-section of 30-nm-deep contact windows etched into the Si by RIE. The dashed line shows the original Si substrate surface. The results of SPE at three different growth stages are shown in the SEM micrographs: (b) the nucleation at the corners and (c) the fast growth at the corners of 1.8 μm × 1.8 μm contact windows, and (d) an entirely filled 1 μm × 1 μm window. In all cases, the growth temperature was 400°C, and the variable growth parameter was the Al/α-Si layer stack overlap of the contact window.

that the surface roughness of PECVD SiO_2 films can be about one order of magnitude larger than that of thermally grown SiO_2.[26] Thus, for such poor-quality oxide, selective deposition in the contact windows can only be achieved if the Al/α-Si layer stack can be patterned with very little overlap of the contact window.

Influence of the Contact Window Surface Treatment

For all the above-described experiments, care was taken not to damage the Si surface of the contact windows by terminating the plasma etching of the windows in oxide with a soft landing on the Si. The significance of this procedure was experimentally investigated by also preparing and analyzing samples where a thermally grown SiO_2 was etched either by a diluted buffered HF solution (1:7), which provides a smooth Si growth interface, or by a trifluoromethane (CHF_3)/hexafluoroethane (C_2F_6)-based reactive-ion etch (RIE) that is known to roughen the surface. With the latter step also a 30-nm-deep cavity was etched into the Si. In both cases, the Si surface was cleaned and the native SiO_2 was removed by a 4-min HF (0.55%) dip-etch. From SEM observations after growth and Al removal, examples of which are presented in Fig. 11, it can be concluded that the damage induced by RIE at the Si growth interface influences neither the nucleation nor the growth.

Geometrical Considerations

If enough α-Si is provided, the growth model given in the previous sections predicts that a large variety of contact window geometries can be filled completely if (1) nucleation on the surrounding oxide is avoided, and (2) the supply of Si to the central regions of the structure is not cut off by too early a filling of the perimeter regions. For an entirely selective deposition in the contact window, the quantity of Si supplied must correspond to the volume of the contact region to be filled. In addition, the temperature-dependent deposition time must be long enough to complete the SPE-Si deposition. Using these guidelines, lines as narrow as 65 nm, which were defined by electron-beam lithography, were successfully filled selectively with high-quality SPE-Si. Also very large structures were filled, such as the ring-shaped contact windows shown in Fig. 12. In this case, the quality of the epitaxial interface was checked by fabricating and characterizing p^+–n diodes. The current–voltage (I–V) characteristics of a 395-μm-long, 1-μm-wide ring diode are shown in Fig. 13 along with those of

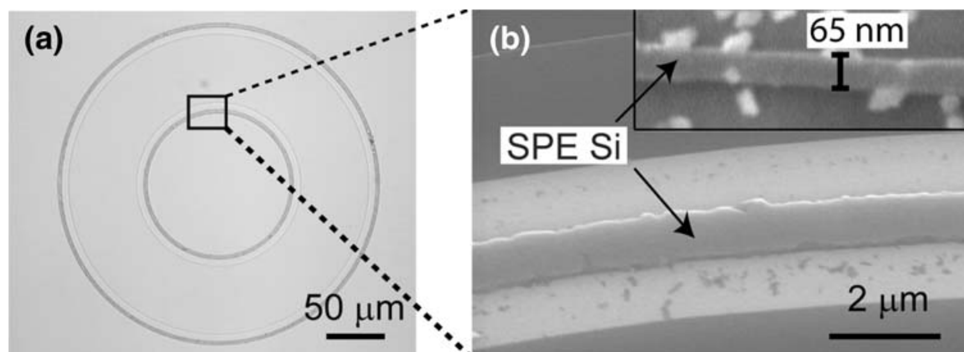

Fig. 12. SPE-Si islands selectively grown in a 395-μm-long 1-μm-wide ring-shaped window. The thicknesses of the Al and α-Si thin films were 100 nm and 75 nm, respectively, and the Al/α-Si island to contact window width ratio was 2. The inset shows a 65-nm-wide electron-beam-defined line-shaped contact window entirely filled in with SPE-Si.

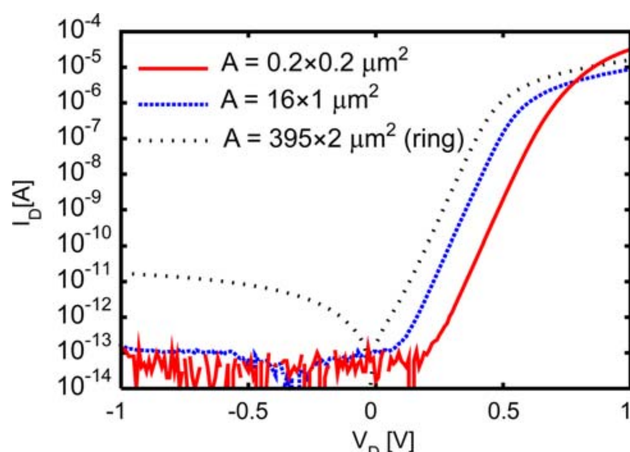

Fig. 13. I–V characteristics of SPE-Si based p^+–n diodes with three different geometries and junction areas.

medium-sized and nanoscale diodes. The same ideality factor ($n \approx 1.05$) is achieved in all cases, with excellent uniformity and reproducibility over the wafers. Thus it can be concluded that the epitaxy is practically defect free in all cases, also at the diode perimeter.

CONCLUSIONS

It has been demonstrated by a multitude of experimental material that the proposed semi-empirical model for the growth mechanisms of Si SPE using Al as a transport layer can predict the selective and complete filling of contact windows to c-Si substrates. In the early growth phase, five specific stages have been distinguished. These are, in order of occurrence: (1) formation of "free" Si at the Al/α-Si interface, (2) diffusion of Si along the Al grain boundaries, (3) nucleation at the Si substrate surface, (4) nuclei rearrangement, and (5) crystal growth.

Two factors that are shown to be important for achieving high-quality material on (100) Si are: (1) the strong preferential growth in the $\langle 100 \rangle$ direction and (2) the fast diffusion of Si through Al grain boundaries and other interfaces. With the model and the much improved understanding of the other process parameters which affect the deposition mechanisms, such as the roughness of the dielectric and Si surfaces, it was possible to predict whether a specific contact window geometry could be filled by a single-crystalline SPE-Si island. Optimized growth parameters were successfully applied to the formation of SPE-Si grown on individual contact window areas up to several hundreds of square microns in size. Confirmation of the high quality of the resulting epitaxial filling of these windows was also obtained electrically by incorporating the SPE islands in p^+–n diodes that showed near-ideal electrical behavior.

ACKNOWLEDGEMENTS

The authors would like to thank the staff of the DIMES-ICP cleanrooms for their continual support. G. Vastola also acknowledges fruitful discussions with Prof. L. Miglio and F. Montalenti. This research is supported by the Dutch Foundation for Fundamental Research on Matter (Stichting FOM) and performed in cooperation with the EU-FP6 project D-DotFET.

OPEN ACCESS

This article is distributed under the terms of the Creative Commons Attribution Noncommercial License which permits any noncommercial use, distribution, and reproduction in any medium, provided the original author(s) and source are credited.

REFERENCES

1. S.W. Lee and S.K. Joo, *IEEE Electron. Dev. Lett.* 17, 160 (1996).
2. O. Nast, S. Brehme, D.H. Neuhaus, and S.R. Wenham, *IEEE Trans. Electron. Dev.* 46, 2062 (1999).
3. C. Spinella and S. Lombardo, *J. Appl. Phys.* 84, 5383 (1998).
4. H. Qingheng, E.S. Yang, and H. Izmirliyan, *Solid Stat Electron.* 5, 1187 (1982).

5. J.Y. Wang, D. He, Y.H. Zhao, and E.J. Mittemeijer, *Appl. Phys. Lett.* 88, 19101 (2006).
6. O. Nast and A.J. Hartmann, *J. Appl. Phys.* 88, 716 (2000).
7. A. Sarikov, J. Schneider, M. Muske, S. Gall, and W. Fuhs, *J. Non-Cryst. Solids* 352, 980 (2006).
8. Y. Civale, L.K. Nanver, P. Hadley, E.J.G. Goudena, and H. Schellevis, *IEEE Electron. Dev. Lett.* 27, 341 (2006).
9. Y. Civale, L.K. Nanver, and H. Schellevis, *IEEE Trans. Nanotechnol.* 6, 196 (2007).
10. Y. Civale, L.K. Nanver, S.G. Alberici, A. Gammon, and I. Kelly, *Electrochem. Solid State Lett.* 11, H74 (2008).
11. J. Schneider, A. Sarikov, J. Klein, M. Muske, I. Sieber, T. Quinn, H.S. Reehal, S. Gall, and W. Fuhs, *J. Cryst. Growth* 287, 423 (2006).
12. A. Hiraki, *Surf. Sci.* 168, 74 (1986).
13. J.A. Thornton, *J. Vac. Sci. Technol.* 11, 666 (1974).
14. D. He, J.Y. Wang, and E.J. Mittemeijer, *Appl. Surf. Sci.* 252, 5470 (2006).
15. D. He, J.Y. Wang, and E.J. Mittemeijer, *J. Appl. Phys.* 97, 93524 (2005).
16. D.W. Pashley, *Adv. Phys.* 14, 327 (1965).
17. J. Tersoff, *Phys. Rev. B.* 38, 9902 (1988).
18. L. Csepregi, E.F. Kennedy, J.W. Mayer, and T.W. Sigmon, *J. Appl. Phys.* 49, 3906 (1978).
19. R. Drosd and J. Washburn, *J. Appl. Phys.* 53, 397 (1982).
20. G. Wulff, *Z. Kristallogr.* 34, 449 (1901).
21. A. Bavard, J. Eymery, A. Pascale, and F. Fournel, *Phys. Status Solidi B* 243, 3963 (2006).
22. Y. Tu and J. Tersoff, *Phys. Rev. Lett.* 84, 4393 (2000).
23. Y. Civale, L.K. Nanver, P. Hadley, H.W. van Zeijl, E.J.G. Goudena, and H. Schellevis. *Proceedings of Materials Research Society Spring Meeting*, San Francisco, CA, USA, 0940-P05-04 (2006).
24. O. Nast and A.J. Hartmann, *J. Appl. Phys.* 88, 716 (2000).
25. O. Nast and S. Wenham, *J. Appl. Phys.* 88, 124 (2000).
26. G. Pandraud, T.M. Koster, C. Gui, M. Dijkstra, A. Van den Berg, and P.V. Lambeck, *Sens. Actuators* 85, 158 (2000).